Progress in the Ground Testing for a Cosmic Dawn Global Spectrum Measurement System

Jiaqin Xu, Shenzhe Xu, Cong Zhang, Jiacong Zhu, and Fengquan Wu

Abstract – Detecting the 21-cm global signal from the cosmic dawn is one of the key science objectives of the Hongmeng cislunar orbit ultralong wavelength array project. This requires a high-precision spectrum measurement system. Here, we report the progress in the development of this system. For the ground testing, which differs from the satellite's free-space environment, a dual-elliptical cylindrical antenna with low-beam chromaticity has been developed, housing the receiver within it. The receiver features a real-time self-calibration system, enabling high-precision spectrum measurement. A set of the devices has been installed at a radio-quiet site, and we present the preliminary results obtained through test observations.

1. Introduction

The redshifted 21-cm signal produced by the neutral hydrogen during the cosmic dawn and epoch of reionization provides a key approach to understanding the early evolution of the universe. The global 21-cm signal, which is an average over the whole sky or large sky area, can be measured with a single, wide-beam antenna in global spectrum experiments. The 21-cm signal can be distinguished from the foreground, which is approximately five orders of magnitude stronger by its spectral features. While the foreground temperature varies smoothly with frequency, the 21-cm signal shows characteristic changes due to different redshifts at each frequency. Thus, the global 21-cm signal can be extracted by measuring the sky spectrum precisely and subtracting the smooth foreground. However, this signal is incredibly faint, with an effective brightness temperature difference ranging from tens to hundreds of millikelvin. As a result, isolating it from foreground radio emissions and instrumental system effects is a significant challenge.

Several global spectrum experiments are currently underway worldwide, including EDGES, SARAS, SCI-HI, HIGH-Z, LEDA, REACH, and MIST [1–5]. Of note, the EDGES team reported the detection of an absorption trough centered at 78 MHz within the frequency range associated with the cosmic dawn [1]. However, the latest SARAS results are inconsistent with this [6], highlighting the need for more precise and independent measurements to eliminate potential systematic errors.

The cislunar orbit, especially the part that is shielded from the radiation of Earth by the Moon, offers an ideal place to make a global 21-cm signal measurement, where many systematic problems in ground-based experiments could be avoided, such as the effect of ground reflection, ionosphere, and radio-frequency interference [7]. The Hongmeng Project is an ongoing lunar orbiting satellite project. The basic idea is that an array of satellites will be launched into the same lunar orbit and make low-frequency observations there [8, 9]. A mother satellite handles the communication with Earth, eight daughter satellites for making interferometric imaging and spectral observations at the low-frequency band below 30 MHz, and another daughter satellite measures the global spectrum above 30 MHz to probe the Cosmic Dawn. This last daughter satellite employs an integrated design combining an "ice cream" (spherical cone) antenna and satellite body [9]. However, directly testing such a satellite antenna on the ground is difficult because when it is mounted in its natural posture, its main beam lobe is pointed toward the horizon plane and susceptible to radio frequency (RF) interference. The ground would also alter its chromaticity characteristics. To address this, we have specifically designed a dual-elliptical cylindrical antenna for ground testing, with the main beam oriented toward the zenith and excellent chromaticity properties. As in the satellite, the receiver electronics are housed inside one of the elliptical cylinders, enabling us to test analogous high-precision receiver systems on the ground.

In the following sections, the design and system architecture of the instrument are described in detail. A prototype has also been built and deployed in a radio-quiet area in Xinjiang for testing.

2. System Design

In global spectrum experiments, to distinguish the 21-cm signal from the foreground, the antenna needs a smooth, frequency-independent beam to avoid convolving sky foreground radiation anisotropies into the spectral structure [10]. Different antenna designs and their corresponding receiver design have been employed in various experiments [11, 12]. Here, we propose to use a dual-elliptical cylindrical antenna. The three-dimensional design of the elliptical cylinder allows the receiver to be directly installed inside the

Manuscript received 6 March 2025. This work was supported by the Chinese Academy of Science Instrument R&D program grant ZDKYYQ20200008, the NSFC grants 12361141814, 12273070, 12473094, 12203061, 12303004.

Jiaqin Xu, Shenzhe Xu, Cong Zhang, Jiacong Zhu, and Fengquan Wu are with National Astronomical Observatories Chinese Academy of Sciences, Beijing 100101, China and the School of Astronomy and Space Science, University of Chinese Academy of Sciences, Beijing 100049, China; e-mail: xujq@bao.ac.cn, wufq@bao.ac.cn.

Table 1. Antenna structural parameters

Parameter	Value
Elliptical cylinder major-minor axis ratio	2.1
Elliptical cylinder minor axis radius	475 mm
Elliptical cylinder thickness	190 mm
Antenna height above ground	850 mm
Distance between elliptical cylinders	76 mm

antenna, eliminating the need for a balun and the associated corrections for balun losses and the complications of transmitting the signal to separate receiver box. The smooth edges of the antenna ensure uniform current flow and consistent beam performance across the 50-MHz to 100-MHz band. This design provides good impedance matching and minimizes signal reflection. The dimensions of the antenna are presented in Table 1. We use FEKO simulation software to simulate the antenna, with an infinite metallic plane serving as a ground plane below the antenna. The beam pattern and the S_{11} parameters of the design are shown in Figure 1.

The receiver features an integrated design, with all components installed within the shielding enclosure of one of the antenna cylinders, which is identical to the one used in the satellite case and also facilitates installation. Figure 2 shows a receiver schematic diagram, including the analog frontend, digital backend, and power supply module. To ensure electromagnetic compatibility of the receiver system and prevent mutual interference among components, the analog and digital components have been placed in separate shielding compartments within the enclosure. To implement a

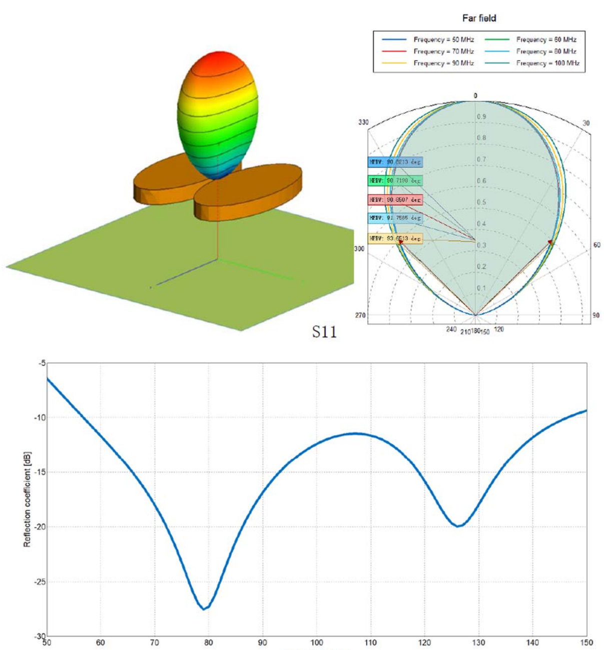

Figure 1. The dual-elliptical cylindrical antenna (top left), its beam pattern (top right), and the S_{11} parameter simulation results.

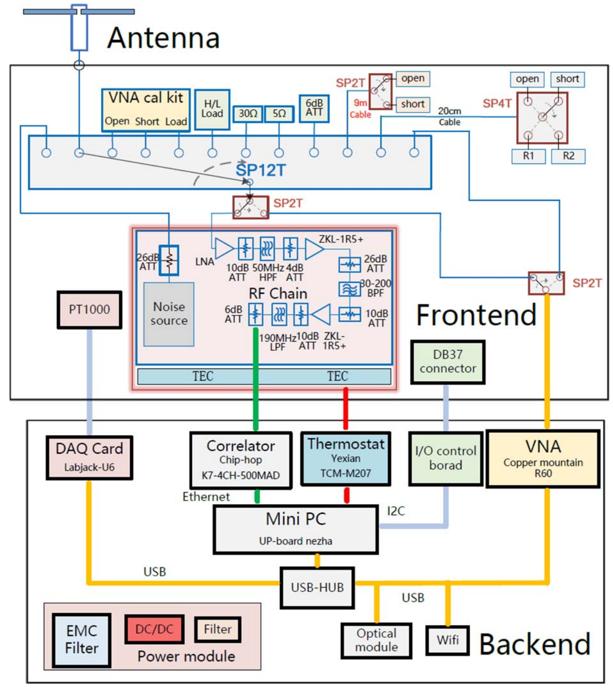

Figure 2. Receiver schematic diagram.

real-time self-calibration function of the measurement system, we designed an RF switch matrix in the analog front end. The antenna and various internal calibration sources are switched to the correlator input channels according to preprogrammed sequences for spectrum measurement, enabling calibration in the postprocessing of the data.

Additionally, the antenna, receiver, and calibrators are also switched to the vector network analyzer measurement channel for reflection coefficient measurement. The active RF devices in the receiver will be installed on a thermostatically controlled plate to improve the stability of the measurement system. Figure 3 shows a photograph of the actual receiver prototype after installation.

3. Receiver Calibration

In global spectrum experiments, internal sources are used to provide high-precision calibration. Figure 4 shows the calibration process of the receiver. The high- or low-temperature load is used for absolute calibration of the temperature scale of the receiver system, which is based on fundamental physics principles. A noise source performs relative calibration on the receiver to eliminate the system gain variation over time. The impedance mismatch between the antenna and receiver must be considered, which generates standing waves within the system. Open-ended and shorted long cables are used to solve the noise parameters of the receiver system. To ensure accuracy, it is necessary to analyze the response of the

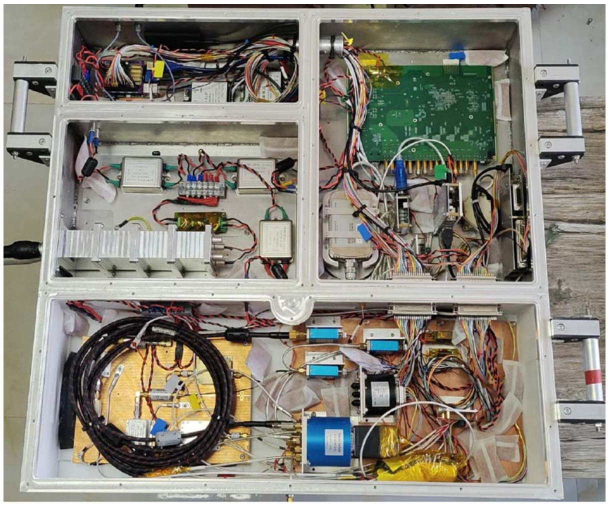

Figure 3. Photograph of a receiver prototype.

receiver, especially to model receiver noise accurately. The noise wave model is used in our analysis [13–16].

$$P_{\rm cal} = g_{\rm sys}[T_{\rm cal}(1 - |\Gamma_{\rm cal}|^2)|F|^2 + T_{\rm unc}|\Gamma_{\rm cal}|^2|F|^2 + T_{\rm cos}{\rm Re}(\Gamma_{\rm cal}F) + T_{\rm sin}{\rm Im}(\Gamma_{\rm cal}F) + T_0], \quad (1)$$

where

$$F = \frac{\sqrt{1 - |\Gamma_{\rm rec}|^2}}{1 - \Gamma_{\rm cal}\Gamma_{\rm rec}}$$

g_{sys} is the receiver gain, T_{cal} is the antenna noise temperature, Γ_{cal} is the reflection coefficient of the antenna, and Γ_{rec} is the reflection coefficient of the receiver. $T_{unc}, T_{cos}, T_{sin}, T_0$ represent uncorrelated noise, cosine-correlated noise, sine-correlated noise, and receiver noise offset, respectively.

Based on the noise wave receiver calibration method, we conducted internal calibration measurements to determine the various parameters in the equation. Figure 5 shows the noise parameters. Here, C_1 and C_2 are the multiplicative and additive calibration coefficients, respectively, which are used to correct the absolute calibration of the receiver [15]. T_u is the uncorrelated noise parameter. T_c and T_s are the sine and cosine noise parameters of the correlated receiver noise, respectively.

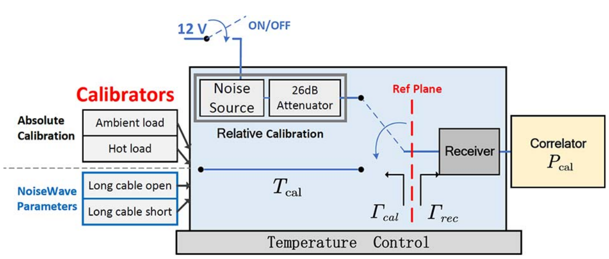

Figure 4. Receiver calibration scheme.

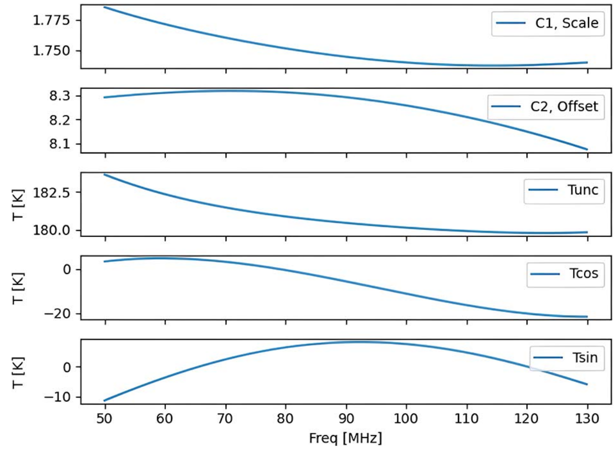

Figure 5. Receiver noise parameters.

To verify the calibration results of the receiver, we use an antenna simulator to check its calibration accuracy. A 30-Ω room-temperature load is used. According to the Nyquist theorem, within the range of normal temperature and low frequencies, their equivalent noise temperature is equal to the ambient physical temperature. The 30-Ω load, when connected to the circuit, has a reflection coefficient close to that of the antenna in our experiment. We measure its physical temperature by attaching a PT1000 temperature probe. The calibration results are shown in Figure 6. When the restored noise temperature of the load is compared with the measured physical temperature, the residual error is less than 0.1 K.

4. Field Measurements

We carried out field observation experiments in a radio-quiet site located at the Hongliuxia Station in Xinjiang, a few kilometers away from the Tianlai experiment site [18]. As shown in Figure 7, a prototype of the measurement system has been installed at the site, surrounded by a rectangular fence made of wood and plastics.

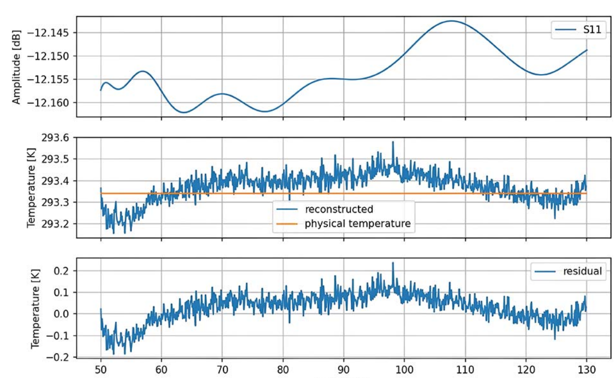

Figure 6. 30-Ω load calibration result.

Figure 7. Measuring system field installation.

The ground of the antenna has a significant impact on the antenna beam [17]. A conventional approach for ground-based experiments is to lay a large, well-grounded conductor net below the antenna so that the antenna can be approximated as being placed on an infinitely large conducting plane.

In our experiment, we prepared the site by first leveling it and then installing a metal ground grid. The schematic diagram of the metal ground grid is shown in Figure 8. The grounding plane of the metal mesh is essentially a square with a side length of 60 m. Some extension strips oriented in the radiation direction have been installed along its edges to mitigate possible standing waves between the antenna and the edges of the grounding mesh. The outermost strips form a 48-m radius circle, and the inner strips have a 42.43-m radius. The mesh size of the grounding mesh is 5 cm. At the center of the ground plane, we initially placed a 2.5-m $\times$ 2.5-m aluminum plate where the antenna mount was installed. However, later, we find that better results can be obtained without the aluminum plate, perhaps because the solid plate generates stronger standing waves near the antenna, and it may also form nonuniform gaps with the mesh.

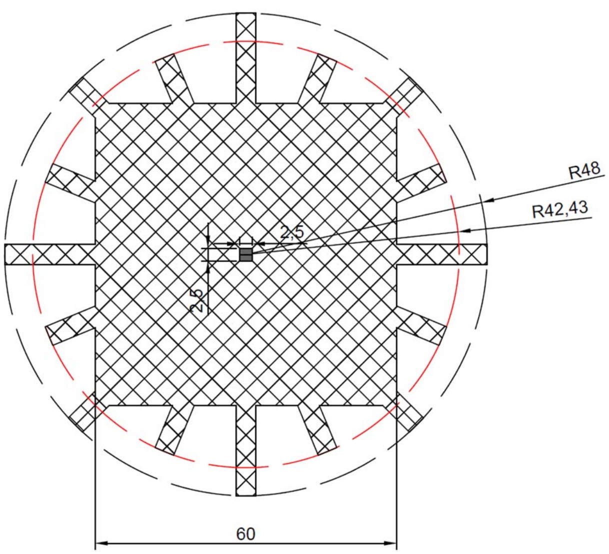

Figure 8. Schematic diagram of the installation of the metal grounding mesh.

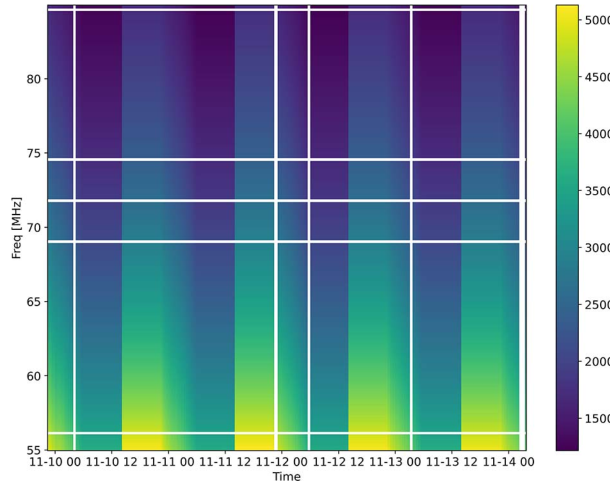

Figure 9. Sky temperature waterfall plot.

In Figure 9, we show the calibrated observation data collected at night from November 10 to November 14, 2024. Absolute calibration was first carried out, followed by environmental RF interference flagging and spectral calibration. After further filtering of the observation data, we integrated the sky data with a duration of 1075 s. The resulting average sky spectrum is shown in the top panel of Figure 10. The sky temperature is 4500 K at 55 MHz and 1500 K at 85 MHz. We then use a sixth-order polynomial to fit the foreground component of the

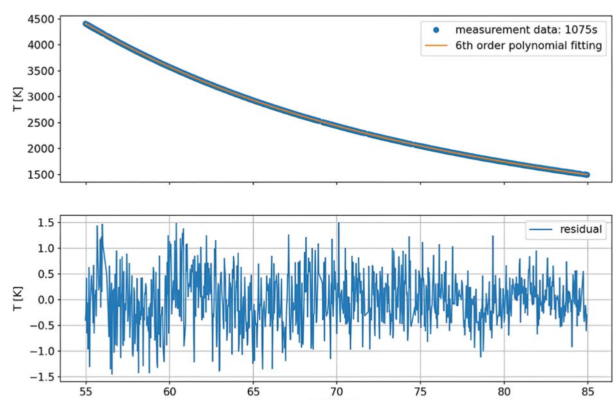

Figure 10. Fifty-five- to 85-MHz sky spectrum and the fitting residuals of the sixth-order polynomial.

sky spectrum, and the residual is less than 1.5 K, as shown in the bottom panel of Figure 10.

5. Discussion and Conclusion

Detecting the global 21-cm signal from the cosmic dawn and epoch of reionization is a challenging observation in the frontier of radio astronomy. In this paper, we introduce a design of our measurement system and present some progress in its field experiment. Preliminary results indicate that it is functioning as expected. After subtracting the sky foreground using a sixth-order polynomial in the frequency range of 55 MHz to 85 MHz, the residual is less than 1.5 K. We are further tuning the experiment and improving its data processing method.

6. Acknowledgment

We thank Nanben Suo, Shijie Sun, Jixia Li, Jiajun Yuan, Haoran Zhang, Juyong Zhang, and Yougang Wang for their help on the experiment, and Furen Deng, Yidong Xu and Xuelei Chen for their discussions.

7. References

1. J. D. Bowman, A. E. E. Rogers, R. A. Monsalve, T. J. Mozdzen, and N. Mahesh, "An Absorption Profile Centred at 78 Megahertz in the Sky - Averaged Spectrum," *Nature*, **555**, 7694, March 2018, pp. 67-70.
2. S. Singh, R. Subrahmanyan, N. Udaya Shankar, M. S. Rao, A. Fialkov, et al., "First Results on the Epoch of Reionization from First Light with SARAS 2," *The Astrophysical Journal Letters*, **845**, 2, August 2017 pp. L12.
3. E. de Lera Acedo, D. I. L. de Villiers, N. Razavi-Ghods, W. Handley, A. Fialkov, et al., "The REACH Radiometer for Detecting the 21-cm Hydrogen Signal From Redshift z 7.5–28," *Nature Astronomy*, **6**, 8, July 2022, pp. 984-998.
4. R. A. Monsalve, C. Altamirano, V. Bidula, R. Bustos, C. H. Bye, et al., "Mapper of the IGM Spin Temperature: Instrument Overview," *Monthly Notices of the Royal Astronomical Society*, **530**, 4, April 2024 pp. 4125-4147.
5. X. Chen, "From a Small Antenna to a Cosmic Dawn," *Nature Astronomy*, **6**, 2022, pp. 887-888.
6. S. Singh, T. J. Nambissan, R. Subrahmanyan, et al., "Astrophysical constraints from the SARAS 3 non - detection of the cosmic dawn sky - averaged 21 - cm signal," *Nature Astronomy*, vol. **6**, pp. 1473-1483, 2022.
7. X. Chen, X. J. Burns, L. Koopmans, L. H. Rothkaehi, J. Silk, et al., "Discovering the Sky at the Longest Wavelengths With Small Satellite Constellations," arXiv: 1907.10853. doi: 10.48550/arXiv.1907.10853
8. X. Chen, J. Yan, L. Deng, F. Wu, L. Wu, et al., "Discovering the Sky at the Longest Wavelengths With a Lunar Orbit Array," *Philosophical Transactions of the Royal Society of London Series A*, **379**, 2188, January 2021, p, 20190566.
9. X. Chen, J. Yan, Y. C, D. Li, W. Fengquan, et al., "Discovering the Sky at the Longest Wavelength Mission−A Pathfinder for Exploring the Cosmic Dark Ages," *Chinese Journal of Space Science*, **43**, 1, January 2023, pp. 43-59.
10. Y. Shi, F. Deng, Y. Xu, F. Wu, Q. Yan, and X. Chen, "Lunar Orbit Measurement of the Cosmic Dawn's 21 cm Global Spectrum," *The Astrophysical Journal*, **929**, 1, April 2022, p. 32.
11. A. E. E. Rogers, *Details of EDGES-3 prototype*, https://dspace.mit.edu/handle/1721.1/154692, 2019.
12. J. Nambissan, T. R. Subrahmanyan, R. Somashekar, N. Shankar, N. Udaya, et al., "SARAS 3 CD/EoR Radiometer: Design and Performance of the Receiver," *arXiv e-prints*, arXiv:2104.01756, 2021.
13. A. E. E. Rogers and J. D. Bowman, "A New Method for Radio Receiver Calibration," *Radio Science*, **47**, 2012, pp. RS0K06.
14. R. P. Meys, "A Wave Approach to the Noise Properties of Linear Microwave Devices," *IEEE Transactions on Microwave Theory and Techniques*, **26**, 1, 1978, pp. 34-37.
15. R. A. Monsalve, A. E. E. Rogers, J. D. Bowman, et al., "Calibration of the Edges High - Band Receiver to Observe the Global 21cm Signature From the Epoch of Reionization," *The Astrophysical Journal*, **835**, 1, January 2017, p. 49.
16. S. Sun, E. de Lera Acedo, F. Wu, B. Yue, J. Zhu, et al., "Calibration Error in 21 - Centimeter Global Spectrum Experiment," *Universe*, **10**, 6, May 2024, p. 236, May 2024.
17. Y. Wang, X. Wang, S. Sun, F. Wu, S. Luo, et al., "Tackling the Challenges in the 21 cm Global Spectrum Experiment: The Impact of Ionosphere and Beam Distortion," *The Astrophysical Journal*, **967**, 87, June 2024.
18. J. Li, S. Zuo, F. Wu, Y. Wang, J. Zhang, et al., "The Tianlai Cylinder Pathfinder Array: System Functions and Basic Performance Analysis," *Science China Physics, Mechanics, and Astronomy*, **63**, September 2020, p. 129862. DOI: 10.1007/s11433-020-1594-8, arxiv:2006.05605.